Publ. Astron. Obs. Belgrade No. 100 (2021), 267 - 273 *Progress Report*

USING BALMER LINES TO UNVEIL THE PRESENCE OF COSMIC RAYS IN THE SUPERNOVA REMNANT SNR 0509-67.5

S. KNEŽEVIĆ[1], G. MORLINO[2], R. BANDIERA[2], S. SCHULZE[3], G. VAN DE VEN[4] and J. C. RAYMOND[5]

[1] *Astronomical Observatory, Volgina 7, 11000 Belgrade, Serbia*
E–mail: sknezevic@aob.rs.

[2] *INAF - Observatorio Astrofisico di Arcetri, Largo E. Fermi 5,I-50125 Firenze, Italy*

[3] *The Oskar Klein Centre, Department of Physics, Stockholm University, AlbaNova, SE-106 91 Stockholm, Sweden*

[4] *Department of Astrophysics, University of Vienna, Türkenschanzstrasse 17, 1180 Vienna, Austria*

[5] *Harvard-Smithsonian Center for Astrophysics, 60 Garden Street, Cambridge, MA, 02138, USA*

Abstract. We present spectroscopic observations of the supernova remnant SNR 0509-67.5 in the Large Magellanic Cloud. We used the integral field-unit MUSE on the Very Large Telescope to spectrally and spatially resolve the fast Balmer shocks around the remnant. We show some preliminary results of the resolved broad Hα-line component, whose width indirectly provides the temperature of the shocked plasma. By coupling this information with the shock speed recently determined by proper motion measurements, we can infer the total amount of energy transformed into cosmic rays in case of their presence. In addition, by comparing monochromatic images of the observed field at various wavelengths, we report a discovery of an object located in the direction of SNR 0509-67.5 that was not observed/reported before.

1. INTRODUCTION

Supernova remnants (SNRs) are widely believed to be the sources of cosmic rays (CRs), the most energetic particles observed on Earth. Direct evidence of CR proton acceleration up to $\sim 10^{15}$ eV energies is still missing, as well as the shock acceleration efficiency, i.e. the amount of energy that SNRs convert into CRs. The acceleration efficiency typically required for SNRs to be the sources of CRs is $\sim 10\%$ (Bykov et al. 2018). In case of efficient acceleration and as a consequence of momentum and energy conservation, the temperature of the plasma behind the shock should be lower than in the case of no acceleration. Moreover, the dynamical reaction of accelerated particles on the background plasma induces the formation of a precursor upstream of the shock (see e.g. Malkov & Drury 2001).

Collisionless shocks propagating through a partially neutral interstellar medium (ISM) have a characteristic spectral signature in the form of Balmer lines among which the Hα line is the brightest. Its characteristic double-component profile reveals

the conditions in the ISM and the shock itself. Post-shock protons interact with pre-shock neutrals overrun by the shock in two ways. In the process of excitation a narrow-line component (width $\sim 10\,\mathrm{km\,s^{-1}}$ reflecting the temperature in front of the shock) is produced, while a broad component (width $\sim 1000\,\mathrm{km\,s^{-1}}$ corresponding to the temperature of immediate post-shock protons[1]) is produced in charge-exchange process (Chevalier & Raymond 1978). The width of the broad component can be used to infer the shock acceleration efficiency, while the width of the narrow component and the narrow-to-broad intensity ratio provide the information on the maximum energy of accelerated particles and the amount of CR heating in the shock precursor (Blasi et al. 2012, Morlino et al. 2012, Morlino et al. 2013).

Some Balmer SNRs seem to be efficient CR accelerators. One of them is SNR 0509-67.5 in the Large Magellanic Cloud (LMC) that shows indication of particle acceleration in the southwestern (SW) region (Smith et al. 1994, Helder et al. 2010). The distance to the LMC is well known and proper motion studies (Hovey et al. 2015) measured the average shock speed of $6500 \pm 200\,\mathrm{km\,s^{-1}}$ (with a peak speed of around $8000\,\mathrm{km\,s^{-1}}$ at some positions). Having an independent shock velocity estimate makes the SNR 0509-67.5 a good candidate for studying CR acceleration, since we know what broad-component widths we can expect in CR absence scenario.

2. DATA ANALYSIS AND RESULTS

2. 1. OBSERVATIONS & DATA REDUCTION

Previous studies (Helder et al. 2010) used long slits to extract profiles from two locations in SNR 0509-67.5. Those observations lack the sensitivity to detect the very faint broad component in the northeastern (NE) region and the spectrum in the SW rim covered the region of multiple shock filaments with different speeds which interpretation cannot unambiguously point towards CR acceleration. Here we present observations with the Multi Unit Spectroscopic Explorer (MUSE) instrument at the ESO Very Large Telescope that we obtained in November and December 2017 and January 2018 (total integration time of 3 hours and good seeing conditions of $1''$). MUSE's large field of view (FOV) of $1' \times 1'$ covers the entire SNR 0509-67.5 (diameter $\approx 30''$). Thanks to its high spatial resolution of $0.2''$/pix, we can trace different shock filaments and resolve the geometric effects. MUSE's high sensitivity enables detection of very faint broad component in the NE rim. The narrow component cannot be resolved with the MUSE spectral resolution power of 3000 at Hα. The spectral range covered was 4750-9350 Å.

The data were reduced using the MUSE pipeline recipes version 2.4.2 and following the standard reduction procedure. We did not take sky exposures, but created a sky model from the region free from remnant (including its interior) and stellar emission. This region was further sampled so that only the faintest parts were used by the pipeline for sky model estimation. The entire FOV is crowded with stars (Figure 1) whose emission affects spectra at some locations on the remnant. To clean the spectral features of the stars on the observed Hα-line profiles, we applied the following stellar subtraction method. We created two off-line stellar images collapsing the

[1]For a gas emitting a thermal, Gaussian-shaped line, the line width relates to the temperature as $W \sim T^{1/2}$. The shock heats up the impacted material to a temperature $T \sim V_{\mathrm{sh}}^2$ (jump conditions). For the assumption of a monoatomic, non-relativistic gas the broad-component width relates to the shock speed as $W \sim V_{\mathrm{sh}}$.

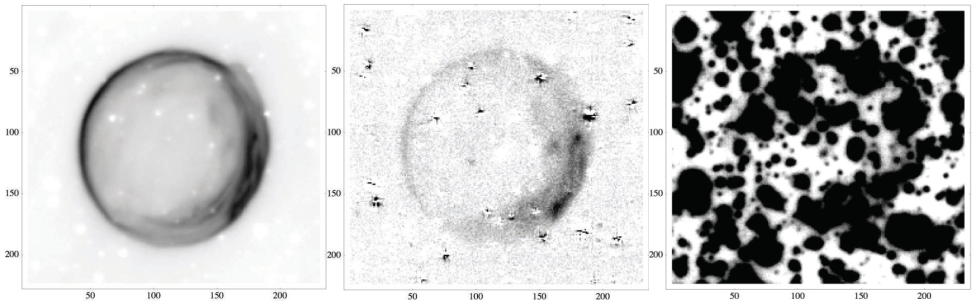

Figure 1: MUSE observations of SNR 0509-67.5: narrow-component map (left), broad-component map (middle) and broad component before stellar subtraction (right).

datacube around certain wavelength (velocity) channels; one from -20 000 km s^{-1} to -8000 km s^{-1} and the other from 8000 km s^{-1} to 20 000 km s^{-1} (the narrow Hα component is centered at zero velocity). The ranges were chosen to avoid the contamination from the broad Hα component. To minimize biases due to the presence of remnant's emission we have masked out all pixels in the area occupied by the SNR. Every datacube channel was then fitted with a linear combination of the two stellar images plus a constant, where χ^2 minimization was done over all unmasked pixels. Coefficients of stellar images contribution were smoothed by a second-order polynomial fits applied to their wavelength trends excluding 20% of the coefficients deviating the most from the fits. The so-created sky- and stellar-subtracted datacube is used further in the analysis.

2. 2. RESULTS ON SNR 0509-67.5

The geometry of the NE rim shows an almost perfect spherical symmetry. We extracted line profiles (Figure 2) from 0.2″ wide circular arcs in the region with position angle in the range (45°, 105°) and distance from the remnant's center in the range (13.6″, 15.7″). We fit double-Gaussian profiles to the Hα profiles and extract surface brightness, width of the broad component, and its offset with respect to the narrow-component centroid. In order to explain the radial profiles of the observables, we have used the following geometric model: the emission is confined to a spherical thin shell located at a radial distance $r_{\rm sh}$ from the remnant's center. The broad-line component is modelled taking into account the thermal velocity dispersion ($\sigma_{\rm vel}$) and the radial bulk velocity ($V_{\rm bulk}$) of the shocked medium. Finally, the model allows for a gradient of the logarithm of the neutral density in the ambient medium. The best fit solution is found for $r_{\rm sh} \approx 15.4''$, $\sigma_{\rm vel} \approx 1500$ km s^{-1}, $V_{\rm bulk} \approx 3000$ km s^{-1} and a density gradient with components $+6.5 r_{\rm sh}^{-1}$ in the projected radial direction and $-0.85 r_{\rm sh}^{-1}$ along the line-of-sight. This suggests that a strong local gradient of neutrals in the NE rim is present. The post-shock bulk velocity is ≈ 3000 km s^{-1} that, following the classical jump relations for a strong shock, would imply a shock velocity ≈ 4000 km s^{-1}, smaller than that derived from proper motions. We need to further investigate whether this smaller speed might be a consequence of the velocity dependence on charge-exchange processes so that the mean velocity of neutrals, the ones created in these processes and responsible for the production of broad component, may be significantly different from that of the ions.

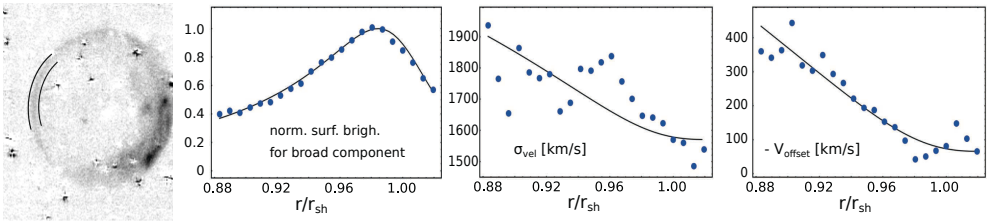

Figure 2: Geometry of the NE rim. Selected region at position angles (45°,105°) and radius (13.6″, 15.7″) from where the line profiles of 0.2″ wide circular arcs were extracted (first panel). Radial profiles of the measured broad-component surface brightness, width and its offset from the narrow-component centroid (second, third and fourth panels). Blue dots are data and black line is the best-fit model.

In addition to profiles in the NE rim, we mapped the Hα profiles all around the remnant at the locations for which the proper motion was measured and presented in the paper Hovey et al. (2015). For the known heliocentric distance of 50 ± 1 kpc to the LMC, these authors estimate a shock velocity of $\approx 6500\,\mathrm{km\,s^{-1}}$ on average all around the remnant. In the left panel of Figure 3 we show a spectrum from nearly the same location in the NE region as observed by Helder et al. (2010) using long slit where the broad component was not resolved. We show that the MUSE data resolved the broad line (FWHM = 3740 ± $210\,\mathrm{km\,s^{-1}}$) successfully even though the broad-to-narrow intensity ratio is 0.06. In the middle panel we show the measured broad-line widths as a function of a position angle. We managed to recover 38 out of 44 Hovey et al. (2015) locations (other segments were significantly affected by a nearby star or signal-to-noise (S/N) was very low to resolve broad component). In the right panel we show measured broad-line widths as a function of a shock velocity and

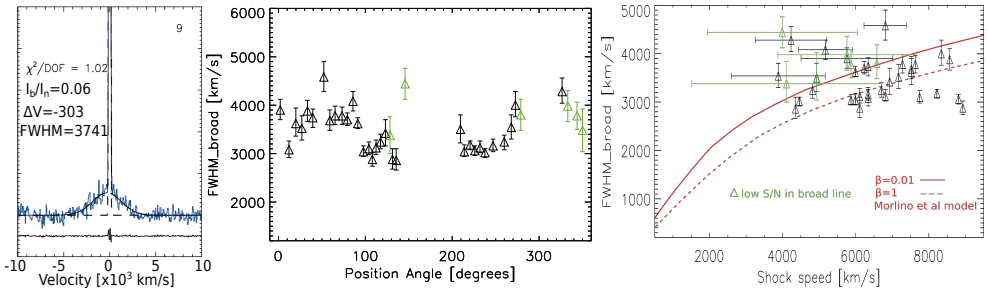

Figure 3: Hα profiles in SNR 0509-67.5. Left panel: spectrum in the NE region (blue line) fitted with double Gaussian (black lines). We measure a broad-to-narrow intensity ratio (I_b/I_n = 0.06 ± 0.01), velocity offset (ΔV = -303 ± $75\,\mathrm{km\,s^{-1}}$) and broad-component width (FWHM = 3740 ± $210\,\mathrm{km\,s^{-1}}$). Middle panel: measured broad-line widths as a function of a position angle. Right panel: measured broad-line widths as a function of a shock velocity together with Morlino et al. (2013) shock model prediction in case of no CRs. Green points are the locations with resolved broad-line component, but with too low S/N to accurately measure parameters.

compare the Morlino et al. (2013) shock model predictions for different electron-to-proton equilibration levels (β), where $\beta = 1$ is full equilibration. The model prediction shown here is without CR acceleration. Any point between the two red lines can be explained without invoking presence of very energetic particles, but the points below the $\beta = 1$ line (dashed line) need some CR physics to be understood. In theory the graph can be populated above the β=0.01 line, but some data points have either uncertain line-parameter estimates or large shock velocity error bars.

2. 3. DETECTION OF A NEW SOURCE

We detected several new sources in the MUSE FOV. One of them is a background object in the SNR field at around RA = 05^{h}:09^{m}:35^{s}.45 and DEC = -67°:31′:15″.02. It is bright at 6333 Å (see Figure 4), but also at 7373 Å, 8258 Å, 8423 Å and 8505 Å (see the spectrum in Figure 5). The object was not previously reported in any catalog. We used Manual and Automatic Redshift Software (Marz; Hinton et al. 2016) to measure the redshift and identify the nature of the object. Before running Marz we cleaned the red part of the spectrum, that is significantly affected by sky residuals, performing principal component analysis with the Zurich Atmosphere Purge (ZAP) code (Soto et al. 2016). Marz uses 12 template spectra: 5 stellar, 6 galactic and 1 AGN template. The best match was found for a high redshift star forming galaxy at redshift 0.69866, where the above mentioned lines 6333 Å, 7373 Å, 8258 Å, 8423 Å, 8505 Å were identified as [OII], Hγ, Hβ, [OIII], [OIII] lines, respectively.

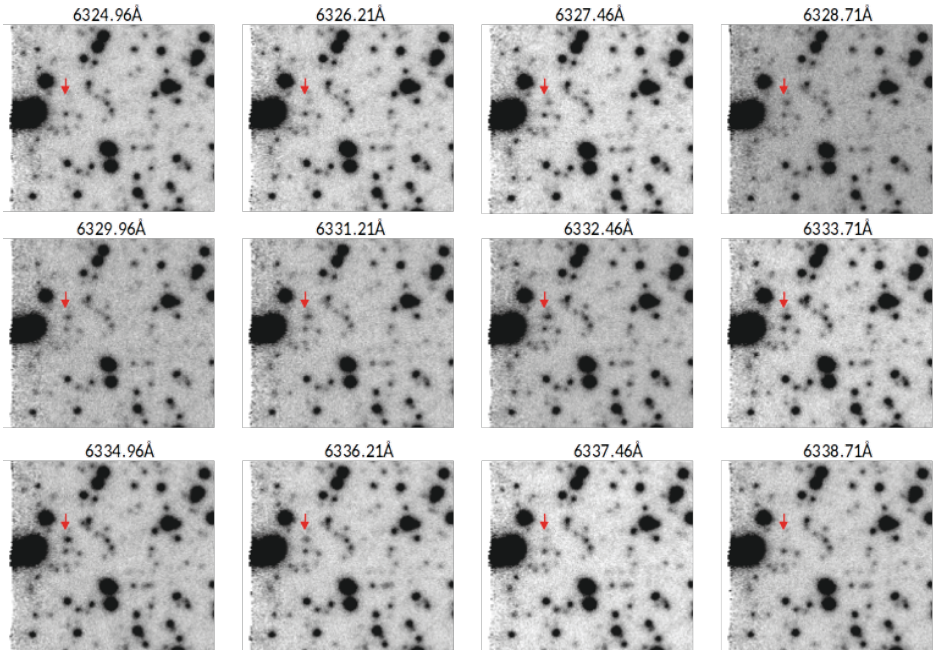

Figure 4: Detected object: Twelve consecutive wavelength-channel images showing the appearance of an object (below the red arrow).

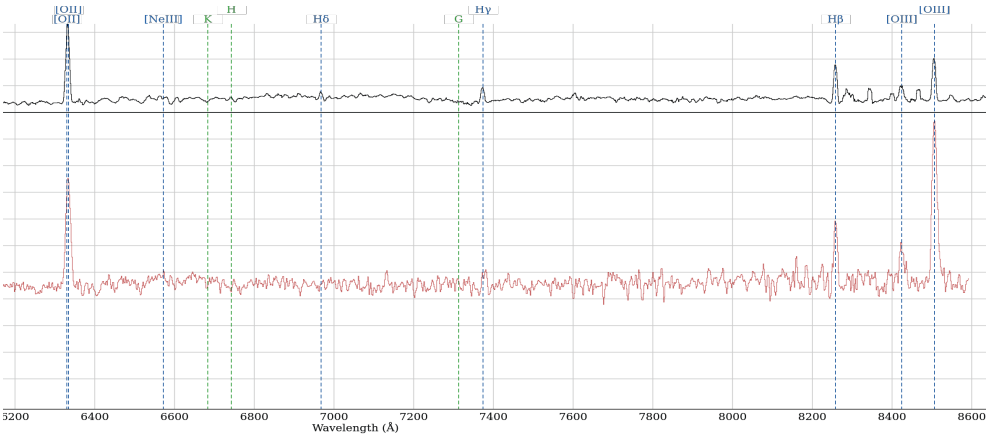

Figure 5: Spectrum of the new source (black line) compared with the template (red line) from Marz software which we used to estimate the redshift and identify the nature of the source. Best match was for high redshift star forming galaxy at z=0.69866.

3. SUMMARY

We presented MUSE observations of the supernova remnant SNR 0509-67.5 in the LMC. Fast Balmer shocks around the remnant were spectrally and spatially resolved due to the instrument's high sensitivity, large FOV and small spatial sampling. We showed the preliminary results of the resolved broad Hα-line component. First results on the shock geometry in the NE region indicate that spherical thin layer model with high neutral density gradients can account for the observed radial trends in the broad-component parameters, but with a lower shock velocity then suggested from proper motions. In addition, we showed that some broad-component widths around the remnant need CR physics to be explained. We are working on combining shock geometry and shock models to interpret the observed line profiles. Finally, we report a discovery of a new object in the FOV that seems to be a galaxy at redshift ≈ 0.7.

Acknowledgements

S. Knežević is supported by the Ministry of Education, Science and Technological Development of the Republic of Serbia through the contract number 451-03-9/2021-14/200002.

References

Blasi, P., Morlino, G., Bandiera, R., Amato, E., Caprioli, D.: 2012, *ApJ*, **755**, 121.
Bykov, A. M., Ellison, D. C., Marcowith, A., Osipov, S. M.: 2018, *Space Sci. Rev.*, **214**, 41.
Chevalier, R. A., Raymond, J. C.: 1978, *ApJ*, **225**, L27.
Helder, E. A., Kosenko, D., Vink, J.: 2010, *ApJ*, **719**, L140.
Hinton, S. R., Davis, T. M., Lidman, C. et al.: 2016, *Astronomy and Computing*, **15**, 61.
Hovey, L., Hughes, J. P., Eriksen, K.: 2015, *ApJ*, **809**, 119.
Malkov, M. A., Drury, L. OC: 2001, *Rep. Prog. Phys.*, **64**, 429.

Morlino, G., Bandiera, R., Blasi, P., Amato, E.: 2012, *ApJ*, **760**, 137.
Morlino, G., Blasi, P., Bandiera, R., Amato, E.: 2013, *ApJ*, **768**, 148.
Smith, R. C., Raymond, J. C., Laming, J. M.: 1994, *ApJ*, **420**, 286.
Soto, K. T., Lilly, S. J., Bacon, R., Richard, J., Conseil, S.: 2016, *MNRAS*, **458**, 3210.